Hindawi
Advances in Condensed Matter Physics
Volume 2022, Article ID 5885992, 7 pages
https://doi.org/10.1155/2022/5885992

Research Article

AlGaN/GaN Heterostructure Schottky Barrier Diodes with Graded Barrier Layer

Honghui Liu,[1] **Zhiwen Liang**,[1] **Chaokun Yan**,[1] **Yuebo Liu**,[2] **Fengge Wang**,[1] **Yanyan Xu**,[1] **Junyu Shen**,[1] **Zhengwen Xiao**,[1] **Zhisheng Wu**,[1] **Yang Liu**,[1] **Qi Wang**,[3] **Xinqiang Wang**,[3,4] **and Baijun Zhang**[1]

[1]*State Key Laboratory of Optoelectronic Materials and Technologies, School of Electronics and Information Technology, Sun Yat-Sen University, Guangzhou 510275, China*
[2]*Science and Technology on Reliability Physics and Application of Electronic Component Laboratory, China Electronic Product Reliability and Environmental Testing Research Institute, Guangzhou 510640, China*
[3]*Dongguan Institue of Opto-Electronics, Peking University, Dongguan 523808, China*
[4]*State Key Laboratory for Mesoscopic Physics and Frontiers Science Center for Nano-Optoelectronics, School of Physics, Peking University, Beijing 100871, China*

Correspondence should be addressed to Baijun Zhang; zhbaij@mail.sysu.edu.cn

Received 29 August 2021; Accepted 21 March 2022; Published 6 April 2022

Academic Editor: Maheswar Nayak

The AlGaN/GaN Schottky barrier diodes (SBDs) working as high-power mixer and multiplier show great potential in millimeter wave (MMW) field owing to their high breakdown voltage. Nevertheless, its further application is severely limited by large reverse leakage current (J_r) since the two-dimensional electron gas (2DEG) channel is hard to be pinched off at low voltage. To address this limitation, a graded AlGaN/GaN heterostructure is introduced to extend the 2DEG channel into a quasi-three-dimensional electron slab. By comparing the fixed Al composition AlGaN/GaN SBD, J_r of the graded AlGaN/GaN SBD is significantly reduced due to the extension of channel carriers, confirming the effective J_r suppression effect of this structure. Furthermore, on this basis, a recessed anode structure is utilized to expect a smaller J_r. The results indicated that the graded AlGaN/GaN SBDs with air-bridge structure have achieved a pretty low J_r value (1.6×10^{-13} A at -15 V), and its cutoff frequency is as high as 60.6 GHz. It is expected that such SBDs with low J_r have significant advantages in future applications.

1. Introduction

The Schottky barrier diodes (SBDs) can be used as mixer and multiplier elements in millimeter wave (MMW) imaging [1, 2], nondestructive testing [3], automotive sensors [4, 5], and communication [6] regions due to their nonlinear effect and mature manufacturing technology [7–11]. To date, the planar GaAs-based SBD is still the most commonly used element, but it always exhibits large reverse leakage currents (J_r) and low breakdown voltage, which seriously limits its applications in the high-power field [9]. By contrast, GaN-based SBDs have a higher breakdown voltage and show greater application advantages in the MMW field. Specifically, some researchers have achieved high breakdown voltage and high cutoff frequency (f_c) with the n^--GaN/n^+-GaN structure [12, 13]. In our previous studies, we also have reported the breakdown voltage of -20 V at 0.1 μA and a f_c of 114 GHz based on AlGaN/GaN heterostructure [14]. Compared to bulk doping, the two-dimensional electron gas (2DEG) with high electron mobility and high carrier concentration can be acquired at AlGaN/GaN interface due to its spontaneous polarization and piezoelectric polarization [15–17]. However, according to related reports, the SBDs based on the AlGaN/GaN heterostructure exhibit large J_r because the 2DEG channel is hard to be pinched off at low voltage [18–21]. To solve this problem, an extended 2DEG structure was designed by the graded AlGaN/GaN heterostructure [22–25]. The graded AlGaN/GaN exhibits high

mobility compared with bulk doping due to the removal of ionized impurity scattering, especially in low-temperature environments [22]. Furthermore, the graded AlGaN/GaN can realize better stability due to the robustness of surface states [24]. However, the characteristics of the graded AlGaN/GaN SBDs are rarely reported, and investigations about leakage properties are still lacking.

In this work, the planar SBDs based on the fixed Al component AlGaN/GaN and the graded AlGaN/GaN heterostructures were fabricated, and their current-voltage (I-V) and capacitance-voltage (C-V) characteristics were evaluated and compared. The carrier distribution of the graded AlGaN/GaN heterostructures was analyzed according to the simulated and experimental results, which supported the extension of the carrier distribution. The forward and reverse currents of SBDs were also studied through the structures with and without recessed anode. As a result, the SBDs with the air-bridge structure have achieved a pretty low J_r value using graded AlGaN/GaN; meanwhile, the f_c is as high as 60.6 GHz.

2. Experiments

The samples of graded AlGaN/GaN heterostructures were grown on a c-plane sapphire substrate by metal-organic chemical vapor deposition (MOCVD). The sample structures consist of a 20 nm AlN nucleation layer, a 2.5 μm C-doped (4×10^{19} cm^{-3}) GaN buffer layer, a 200 nm unintentionally doped (UID) GaN, and a 35 nm graded $Al_{0\sim x}GaN$ barrier layer. C-doped GaN buffer layer is semi-insulating, which avoids the leakage current of the buffer layer and reduces the parasitic capacitance. Si concentration of UID GaN is lower than 10^{16} cm^{-3}. The Al component x of graded $Al_{0\sim x}GaN$ barrier layer from UID GaN to the surface is changed from 0 to 0.27 (S1) and from 0 to 0.35 (S2), as shown in Figure 1(a). In order to compare with the conventional AlGaN/GaN SBDs, a 35 nm fixed Al component $Al_{0.35}Ga_{0.65}N$/GaN heterostructure (S3) was designed, as shown in Figure 1(b). The distribution of Ga and Al composition in the S2 was measured by secondary ion mass spectroscopy (SIMS), as shown in Figure 1(c). It can be seen that the Al composition is graded from UID GaN to $Al_{0.35}Ga_{0.65}N$ surface, which extends the carrier distribution in the channel.

In order to verify the carrier distribution in the graded AlGaN barrier layer, the ring SBDs were fabricated with three steps. (1) The device mesa isolation of 300 nm was performed by dry etching using inductively coupled plasma (ICP). (2) The cathode ohmic metals of Ti/Al/Ni/Au (15/80/20/60 nm) were deposited by E-beam and thermal evaporator followed by rapid thermal annealing (RTA) at 850°C for 30 s in N_2. (3) The metals of Ni/Au (20/80 nm) were deposited in an anode. The schematics of their structures are illustrated in Figures 2(a) and 2(b). In conventional ring SBD, the anode radius (R) is 100 μm, and the space (L_{ac}) between the cathode and anode electrode is 20 μm. In recessed ring SBD, the recess radius (r) is 99 μm, which effectively reduces the capacitance of the ring SBD. Parts of anode metals were designed to be overlapped on the sample surface because the radius of the recess is less than the anode metal. The parallel connection of overlapped planar and recessed sidewall Schottky diode is formed in SBD with the recessed anode. Figure 2(c) shows an optical microscope photograph of ring SBD. The SBD with air-bridge structure was designed to improve f_c. The gold air-bridge which connected the small anode and electrode pad was fabricated using the electroplating technique. The structural parameters of the SBD with air-bridge structure are as follows: $R = 4\,\mu$m, $r = 3.95\,\mu$m, and $L_{ac} = 2\,\mu$m. The reduction of anode size can effectively increase the f_c. Figures 2(d) and 2(e) show the schematic structure and SEM image of the SBD with air-bridge structure, respectively.

The C-V characteristics were measured with alternating voltage of 30 mV amplitude and 1 MHz frequency by Keysight E4980 A LCR meter. The I-V characteristics were tested by Keithley 4200-SCS semiconductor parameter analyzer. All tests were performed at room temperature.

3. Results and Discussion

In order to obtain the characteristics of carrier concentration vs. depth in the graded AlGaN/GaN heterostructure, the C-V characteristics of the conventional ring SBDs and the recessed ring SBDs were measured, as shown in Figures 3(a) and 3(b). It is observed that the capacitance of recessed ring SBDs is reduced by two orders of magnitude compared with the conventional ring SBDs, which is attributed to the sharp reduction of the effective area of the parallel plate capacitor. Theoretically, the capacitance of conventional ring SBD can be described as a parallel plate capacitor with a depletion depth ($W = \varepsilon_0\varepsilon_s A/C$), where ε_0, ε_s, A, and C represent the vacuum dielectric constant, the dielectric constant of AlGaN, the anode area, and the capacitance of reverse-bias junction, respectively. The function of carrier concentration (N_A) vs. depth is described by the following equation [26]:

$$N_A(W) = \frac{1}{d\left(1/C^2\right)/dV} \cdot \frac{2}{q\varepsilon_0\varepsilon_s A^2}, \tag{1}$$

where q is the elementary charge. Based on this, the carrier distributions of S1, S2, and S3 were calculated and plotted in Figure 3(c). For S3, its carrier distribution width is the smallest and is quantified as 1.1 nm, which is much narrower than S1 (5.8 nm) and S2 (6.0 nm). Furthermore, it also has the largest carrier concentration (1.04×10^{20} cm^{-3}) compared to S1 (8×10^{18} cm^{-3}) and S2 (1.37×10^{19} cm^{-3}). As for S1and S2, it can be concluded that their carrier distribution is significantly extended to quasi 3-D electron slab in the graded AlGaN barrier layer. Additionally, the capacitance of S3 is smaller than those of S1 and S2 because the channel carriers are farther away from the anode metal. Consequently, S3 (V_{S3} = -6.5 V) shows a higher pinch-off voltage of depleted channel carriers compared with S1 (V_{S1} = -2.8 V) and S2 (V_{S2} = -3.2 V) owing to the higher carrier concentration and deeper carrier position.

Figure 3(d) shows the band structure versus the depth based on simulation results. The potential well is extended

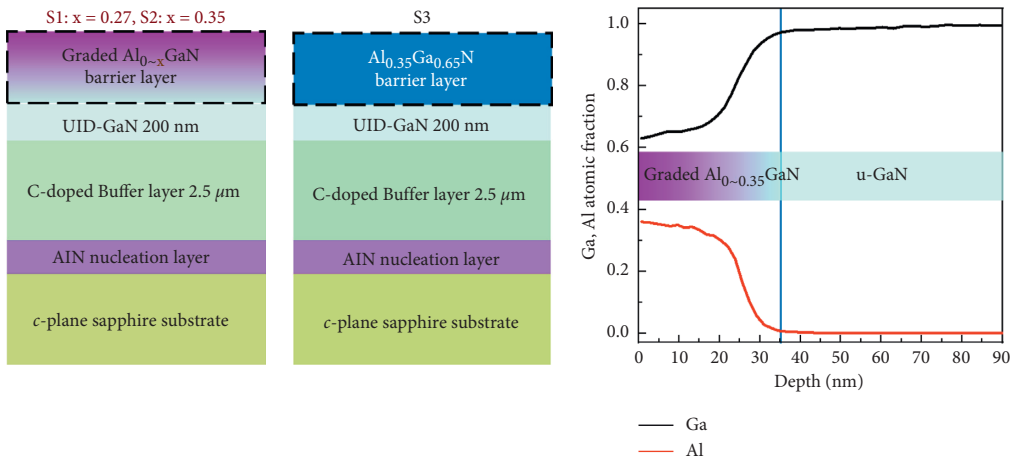

Figure 1: Schematic illustrations of (a) S1 and S2, and (b) S3. (c) Composition of Al and Ga in S2 by SIMS measurement.

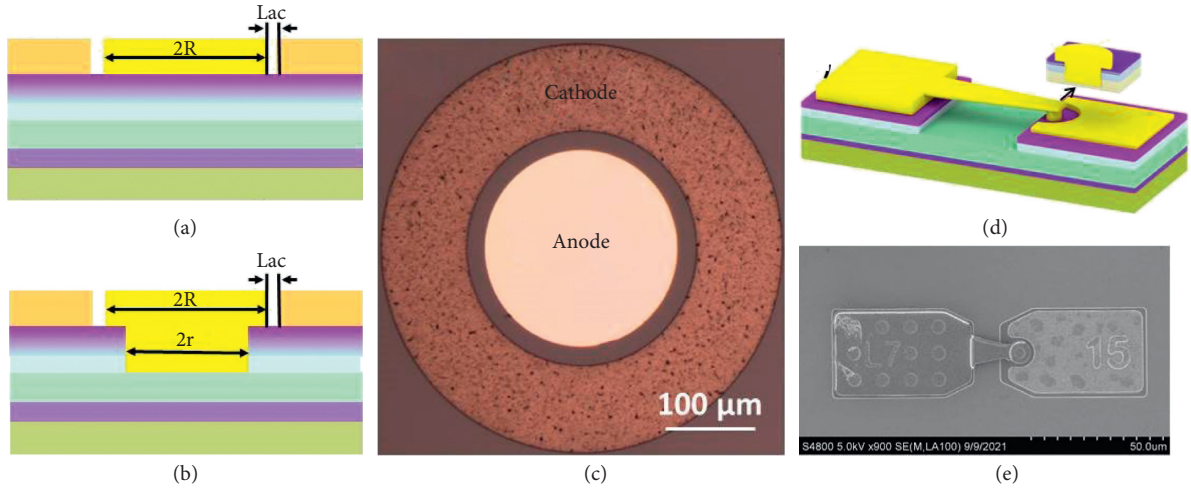

Figure 2: Schematic illustration of (a) conventional and (b) recessed ring SBDs. (c) Optical microscope photograph of ring SBDs. (d) Schematic illustration of the SBD with air-bridge structure. (e) The SEM image of the SBD with air-bridge structure.

from AlGaN/GaN interface to the graded AlGaN barrier layer. Figure 3(c)showsthe carrier distribution versus the depth, which is similar to the carrier distribution by C-V calculation. In order to investigate the extension of the carrier distribution, the distribution of polarization charge along the [0001] direction was calculated by the Poisson equation [27].

$$\nabla \cdot \left[\left(\varepsilon_z + \frac{e_z^2}{c_z} \right) \nabla \varphi \right] = -\rho + \nabla \cdot P_z, \tag{2}$$

where ε_z is permittivity, e_z is the piezoelectric coefficient, c_z is elastic constant, P_z is the total polarization in the material, φ is the electrostatic potential, and ρ is the charge distribution. The parameters of ε_z, e_z, c_z, and P_z are all in [0001] direction. The polarization charge density of the S1 and S2 is significantly reduced by two orders of magnitude compared with S3, demonstrating the extension effect of the graded AlGaN barrier layer on the positive polarization sheet charge at the AlGaN/GaN interface, as shown in Figures 3(e) and 3(f).

Figures 4(a) and 4(b) exhibit good Schottky diode properties of conventional and recessed ring SBDs. When the voltage is lower than the pinch-off voltage ($V_S < V_r < 0$ V), the currents gradually increase as the voltage increases due to the Frenkel-Poole (FP) emission mechanism [21, 28–30], and the channel carriers are not pinch-off at this time. In comparison with the S2 and S3, the S1 increases more slowly due to the thicker barrier width. When the voltage is higher than the pinch-off voltage ($V_r < V_S$), the currents reach saturation thanks to the pinch-off of channel carriers, and in this range, J_r is mainly due to the emission mechanism based on trap-assisted tunneling (TAT). Compared with the fixed Al composition AlGaN/GaN SBD, the saturated J_r of the graded AlGaN/GaN SBD is reduced due to the lower carrier concentration, wider depletion width, and lower tunneling probability. Moreover, the channel is more likely to be pinched off at lower reverse-bias

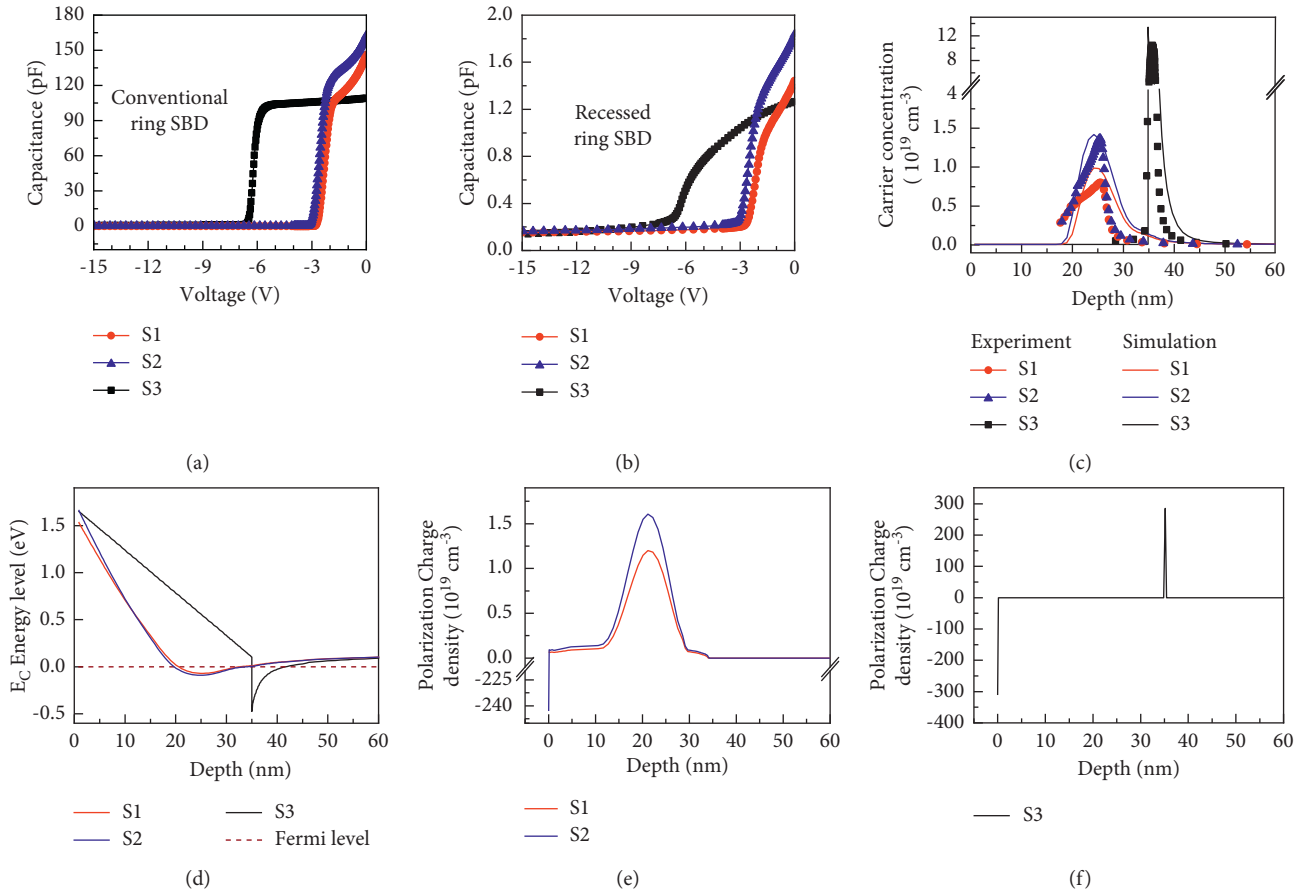

FIGURE 3: The C-V characteristics of (a) conventional and (b) recessed ring SBDs. (c) The carrier concentration vs. depths of S1, S2, and S3 by experiment and simulation. (d) The E_C energy level vs. depths of S1, S2, and S3. The distribution of polarization charge of (e) S1 and S2, and (f) S3.

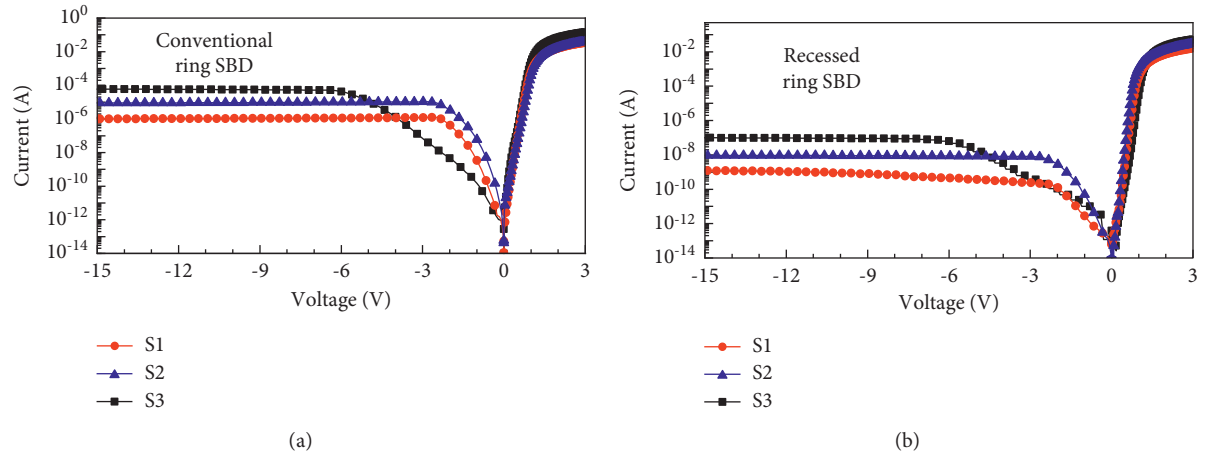

FIGURE 4: The I-V characteristics of (a) conventional and (b) recessed ring SBDs.

voltage due to shallow carrier distribution. In addition, we found that the saturated J_r values are a linear relationship with the effective anode area and are related to the trap concentration on the AlGaN surface [21]. In comparison with conventional rings SBDs, the saturated J_r values of recessed rings SBDs are reduced by about three orders of magnitude, which is contributed to the smaller effective anode area.

The electrical characteristics are summarized in Table 1. The ideality factor of SBDs is larger than 1, which indicates that the transport mechanisms include TAT, recombination, and thermionic emission (TE) under the forward voltage

Table 1: Electrical characteristics of SBDs.

Size (μm)	Sample	Ideality factor	Series resistance (Ω)	Saturated J_r at -15V (A)	Capacitance at 0 V	Cutoff frequency (GHz)
$R = 100$, $r = 0$	S1	1.64	51.5	1.0×10^{-6}	146 pF	0.021
	S2	1.68	39.4	8.8×10^{-6}	163 pF	0.025
	S3	1.53	21.5	5.9×10^{-5}	109 pF	0.067
$R = 100$, $r = 99$	S1	1.34	105.8	1.2×10^{-9}	1.44 pF	1.04
	S2	1.33	52.7	2.0×10^{-8}	1.84 pF	1.66
	S3	1.95	20.5	9.9×10^{-8}	1.25 pF	6.26
$R = 4$, $r = 3.95$	S1	1.89	368	1.6×10^{-13}	10.4 fF	41.7
	S2	1.94	210	1.9×10^{-12}	12.5 fF	60.6
	S3	2.19	151	3.4×10^{-10}	11.5 fF	91.6

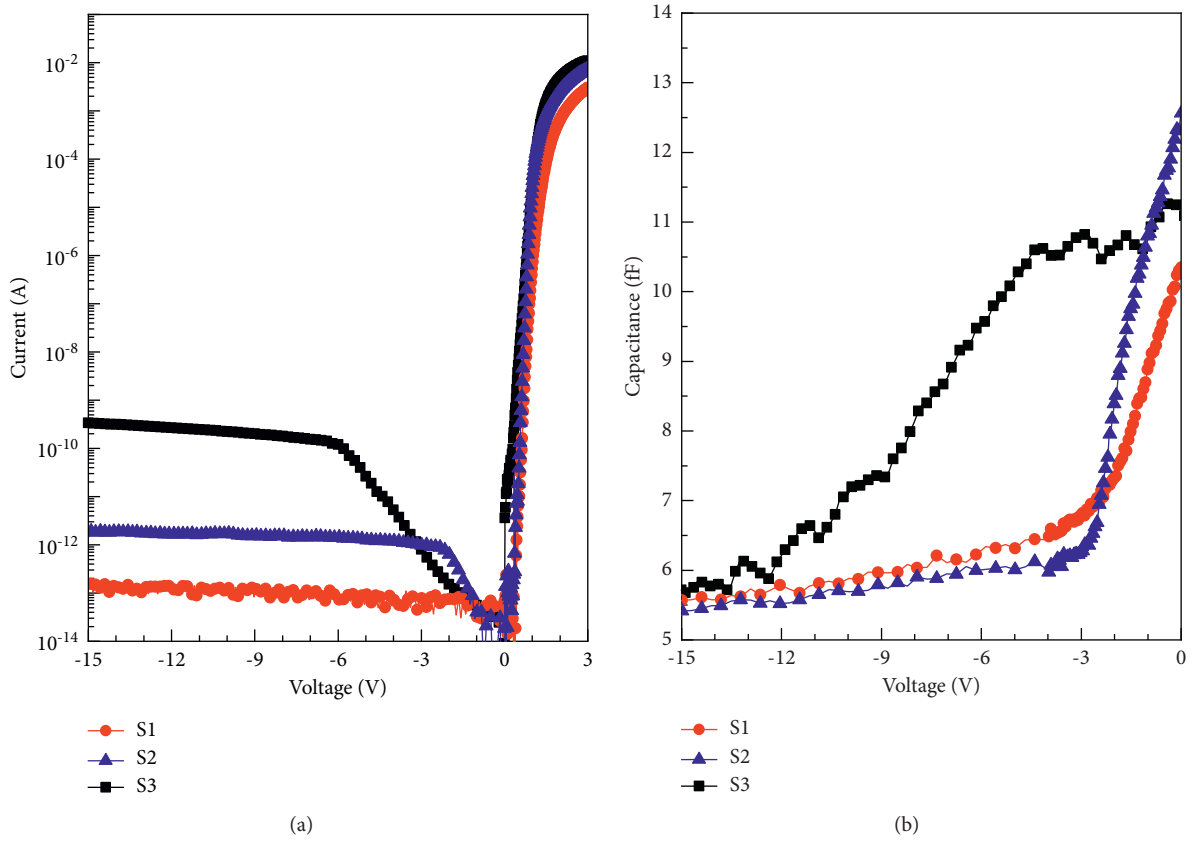

Figure 5: The (a) I-V and (b) C-V characteristics of the air-bridge structure planar SBDs.

[31–33]. The series resistance (R_s) of recessed ring SBDs is larger than conventional ring SBDs because the electrons laterally flow to the anode metal of the recessed sidewall. In comparison with conventional rings SBDs, the f_c of the recessed rings SBDs is improved by two orders of magnitude, as shown in Table 1.

The f_c of SBD is a very important parameter in MMW regions, which is defined as $f_c = 1/(2\pi R_s C_0)$ [34]. The reduction of R_s or C_0 is the only way to improve the f_c. In order to obtain a higher f_c, the SBD with an air-bridge structure is designed. The C-V and I-V characteristics are shown in Figures 5(a) and 5(b), respectively, which exhibit good Schottky diode properties. The value of the J_r between the two pads is about 2.8×10^{-14} A. The electrical characteristics are described in Table 1. In comparison with the SBD of S3, the J_r value of S2 is reduced by two orders of magnitude due to the extension of carriers in the channel. The capacitance of S3 is slowly decreased due to the sidewall capacitance of the recessed SBD device, as shown in Figure 5(b). The S2-based SBD with air-bridge structure shows R_s of 210 Ω, C_0 of 12.5 fF, f_c of 60.6 GHz, and J_r of 1.9×10^{-12} A at -15 V.

The J_r of the air-bridge structure planar SBDs is summarized in Figure 6. Compared with traditional GaAs-based SBDs, the GaN-based SBDs show a much higher breakdown voltage. What's more, the AlGaN/GaN SBDs show lower J_r values. In this work, the graded AlGaN/GaN SBDs with the air-bridge structure have achieved the lowest J_r values of 1.6×10^{-13} A at -15 V, which can effectively reduce the heating of the device in mixer and multiplier.

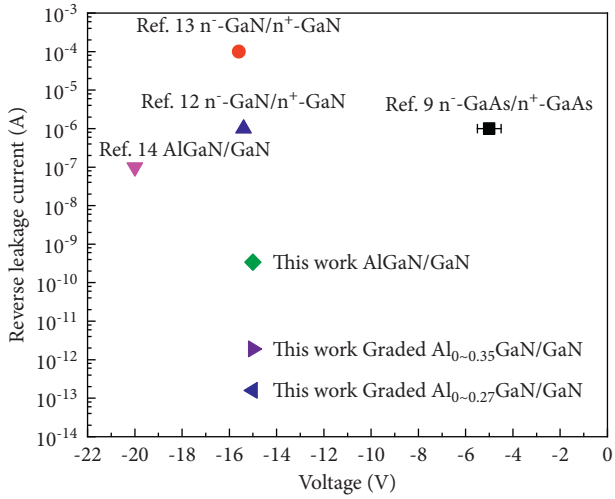

FIGURE 6: The J_r values of the air-bridge structure planar SBDs.

4. Conclusions

In summary, the characteristics of the graded AlGaN/GaN SBDs with and without recessed anode have been evaluated by the I-V and C-V. The carrier distribution of the graded AlGaN/GaN heterostructures was analyzed using the Poisson equation, which reveals the reasons for the extension of the carrier distribution. Compared with the fixed Al component AlGaN/GaN SBD, the J_r is reduced by two orders of magnitude due to the extension of the carrier distribution. The graded AlGaN/GaN SBDs with air-bridge structure have achieved a pretty low J_r value (1.6×10^{-13} A at -15 V). The f_c of graded $Al_{0\sim0.35}GaN/GaN$ SBD with air-bridge structure is 60.6 GHz, and the J_r is as small as 1.9×10^{-12} A at -15 V. These are beneficial to the applications of MMW in the future.

Data Availability

The data that were used to support this study are included within the article.

Conflicts of Interest

The authors declare that there are no conflicts of interest to disclose.

Acknowledgments

This work was partially supported by the Science and Technology Plan of Guangdong Province, China (Grant nos. 2019B010132003 and 2019B010132001), the joint funding of the Nature Science Foundation of China and the Macao Science and Technology Development Fund of China (Grant no. 62061160368), the National Key Research and Development Program (Grant nos. 2016YFB0400105 and 2017YFB0403001), and the Zhuhai Key Technology Laboratory of Wide Bandgap Semiconductor Power Electronics, Sun Yat-sen University, China (Grant no. 20167612042080001).

References

[1] L. Yujiri, M. Shoucri, and P. Moffa, "Passive millimeter-wave imaging," *IEEE Microwave Magazine*, vol. 4, no. 3, pp. 39–50, 2003.

[2] D. M. Sheen, D. L. McMakin, and T. E. Hall, "Three-dimensional millimeter-wave imaging for concealed weapon detection," *IEEE Transactions on Microwave Theory and Techniques*, vol. 49, no. 9, pp. 1581–1592, 2001.

[3] S. Kharkovsky and R. Zoughi, "Microwave and millimeter wave nondestructive testing and evaluation - overview and recent advances," *IEEE Instrumentation and Measurement Magazine*, vol. 10, no. 2, pp. 26–38, 2007.

[4] J. Hasch, E. Topak, R. Schnabel, T. Zwick, R. Weigel, and C. Waldschmidt, "Millimeter-wave technology for automotive radar sensors in the 77 GHz frequency band," *IEEE Transactions on Microwave Theory and Techniques*, vol. 60, no. 3, pp. 845–860, 2012.

[5] J. Choi, V. Va, N. Gonzalez-Prelcic, R. Daniels, C. R. Bhat, and R. W. Heath, "Millimeter-wave vehicular communication to support massive automotive sensing," *IEEE Communications Magazine*, vol. 54, no. 12, pp. 160–167, 2016.

[6] W. Roh, J.-Y. Seol, J. Park et al., "Millimeter-wave beamforming as an enabling technology for 5G cellular communications: theoretical feasibility and prototype results," *IEEE Communications Magazine*, vol. 52, no. 2, pp. 106–113, 2014.

[7] U. R. Pfeiffer, C. Mishra, R. M. Rassel, S. Pinkett, and S. K. Reynolds, "Schottky barrier diode circuits in silicon for future millimeter-wave and terahertz applications," *IEEE Transactions on Microwave Theory and Techniques*, vol. 56, no. 2, pp. 364–371, 2008.

[8] T. W. Crowe, J. L. Hesler, R. M. Weikle, and S. H. Jones, "GaAs devices and circuits for terahertz applications," *Infrared Physics & Technology*, vol. 40, no. 3, pp. 175–189, 1999.

[9] W. L. Bishop, K. Mckiney, R. J. Mattauch, T. W. Crowe, and G. Green, "A novel whiskerless Schottky diode for millimeter and submillimeter wave application," *IEEE MTT-S International Microwave Symposium Digest (Cat. No.87CH2395-2)*, vol. 2, pp. 607–610, 1987.

[10] S. Xiao, T. Wang, T. Liu, C. Zhou, X. Jiang, and J. Zhang, "Active metamaterials and metadevices: a review," *Journal of Physics D-Applied Physics*, vol. 53, no. 50, Article ID 503002, 2020.

[11] Y. Liu, W. Yao, and H. Liu, "Multi-channel AlGaN/GaN Schottky barrier diodes with a half through-hole," *Materials Science in Semiconductor Processing*, vol. 133, Article ID 105934, 2021.

[12] S. Liang, X. Zhang, Y. Lv et al., "A 177-183 GHz high-power GaN-based frequency doubler with over 200 mW output power," *IEEE Electron Device Letters*, vol. 41, no. 5, pp. 669–672, 2020.

[13] B. Zhang, D. Ji, D. Fang, S. Liang, Y. Fan, and X. Chen, "A novel 220-GHz GaN diode on-chip tripler with high driven power," *IEEE Electron Device Letters*, vol. 40, no. 5, pp. 780–783, 2019.

[14] L. Yang, W. Yao, and Y. Liu, "Low capacitance AlGaN/GaN based air-bridge structure planar Schottky diode with a half through-hole," *AIP Advances*, vol. 10, no. 4, Article ID 045219, 2020.

[15] L. Hsu and W. Walukiewicz, "Electron scattering mechanisms at polar GaN/AlGaN interfaces," *Ultrafast Phenomena in Semiconductors Vi*, vol. 4643, pp. 148–162, 2002.

[16] E. T. Yu, X. Z. Dang, P. M. Asbeck, S. S. Lau, and G. J. Sullivan, "Spontaneous and piezoelectric polarization effects in III-V

nitride heterostructures," *Journal of Vacuum Science & Technology B: Microelectronics and Nanometer Structures*, vol. 17, no. 4, pp. 1742–1749, 1999.

[17] O. Ambacher, J. Smart, J. R. Shealy et al., "Two-dimensional electron gases induced by spontaneous and piezoelectric polarization charges in N- and Ga-face AlGaN/GaN heterostructures," *Journal of Applied Physics*, vol. 85, no. 6, pp. 3222–3233, 1999.

[18] W. J. Ha, S. Chhajed, and S. J. Oh, "Analysis of the reverse leakage current in AlGaN/GaN Schottky barrier diodes treated with fluorine plasma," *Applied Physics Letters*, vol. 100, no. 13, Article ID 132104, 2012.

[19] X. Y. Liu, S. X. Zhao, and L. Q. Zhang, "AlGaN/GaN MIS-HEMTs with AlN gate dielectric grown by thermal ALD technique," *Nanoscale Research Letters*, vol. 10, Article ID 109, 2015.

[20] T. Sun, X. Luo, J. Wei, C. Yang, and B. Zhang, "Theoretical and experimental study on AlGaN/GaN Schottky barrier diode on Si substrate with double-heterojunction," *Nanoscale Research Letters*, vol. 15, no. 1, Article ID 149, 2020.

[21] Y. Yao, J. Zhang, and Y. Zheng, "Current transport mechanism of AlGaN/GaN Schottky barrier diode with fully recessed Schottky anode," *Japanese Journal of Applied Physics*, vol. 54, no. 1, Article ID 011001, 2015.

[22] D. Jena, S. Heikman, D. Green et al., "Realization of wide electron slabs by polarization bulk doping in graded III-V nitride semiconductor alloys," *Applied Physics Letters*, vol. 81, no. 23, pp. 4395–4397, 2002.

[23] Y. Fang, Z. Feng, C. Li et al., "Trap behaviors in AlGaN/GaN based polarization-doped field effect transistors by frequency-dependent conductance-voltage characterizations," *Superlattices and Microstructures*, vol. 82, pp. 201–206, 2015.

[24] Y. Fang, Z. Feng, J. Yin et al., "AlGaN/GaN polarization-doped field-effect transistors with graded heterostructure," *IEEE Transactions on Electron Devices*, vol. 61, no. 12, pp. 4084–4089, 2014.

[25] S. Rajan, H. Xing, S. DenBaars, U. K. Mishra, and D. Jena, "AlGaN/GaN polarization-doped field-effect transistor for microwave power applications," *Applied Physics Letters*, vol. 84, no. 9, pp. 1591–1593, 2004.

[26] J. Hilibrand and R. D. Gold, "Determination of the impurity distribution in junction diodes from capacitance-voltage measurements," *RCA Review*, vol. 21, pp. 245–252, 1960.

[27] B. Jogai, J. D. Albrecht, and E. Pan, "Effect of electromechanical coupling on the strain in AlGaN/GaN heterojunction field effect transistors," *Journal of Applied Physics*, vol. 94, no. 6, pp. 3984–3989, 2003.

[28] H. Zhang, E. J. Miller, and E. T. Yu, "Analysis of leakage current mechanisms in Schottky contacts to GaN and Al0.25Ga0.75N/GaN grown by molecular-beam epitaxy," *Journal of Applied Physics*, vol. 99, no. 2, Article ID 023703, 2006.

[29] J. H. Shin, J. Park, S. Jang, T. H. Jang, and K. S. Kim, "Gate metal dependent reverse leakage mechanisms in AlGaN/GaN Schottky diode," *Japanese Journal of Applied Physics*, vol. 52, no. 7, Article ID 70203, 2013.

[30] E. Arslan, S. Butun, and E. Ozbay, "Leakage current by Frenkel-Poole emission in Ni/Au Schottky contacts on Al0.83In0.17N/AlN/GaN heterostructures," *Applied Physics Letters*, vol. 94, no. 14, Article ID 142106, 2009.

[31] M. Grundmann, R. Karsthof, and H. von Wenckstern, "Interface recombination current in type II heterostructure bipolar diodes," *ACS Applied Materials & Interfaces*, vol. 6, no. 17, pp. 14785–14789, 2014.

[32] D. Yan, J. Jiao, J. Ren, G. Yang, and X. Gu, "Forward current transport mechanisms in Ni/Au-AlGaN/GaN Schottky diodes," *Journal of Applied Physics*, vol. 114, Article ID 144511, 2013.

[33] S. Kotzea, A. Debald, M. Heuken, H. Kalisch, and A. Vescan, "High-mobility GaN-on-sapphire p-n diodes with near-unity ideality factor and large breakdown voltage," *Journal of Physics D: Applied Physics*, vol. 52, Article ID 285101, 2014.

[34] K. S. Champlin and G. Eisenstein, "Cutoff frequency of submillimeter Schottky-barrier diodes," *IEEE Transactions on Microwave Theory and Techniques*, vol. 26, no. 1, pp. 31–34, 1978.